JACS
JOURNAL OF THE AMERICAN CHEMICAL SOCIETY
pubs.acs.org/JACS
Article

Regulating the Structures of Self-Assembled Mechanically Interlocked Moleculecular Constructs via Dianion Precursor Substituent Effects

Xu-Lang Chen, Yun-Jia Shen, Chao Yang, Jian-Gao Yang, Xin Sun, Xin Zhang, Yu-Dong Yang, Gong-Ping Wei, Jun-Feng Xiang, Jonathan L. Sessler,* and Han-Yuan Gong*

Cite This: J. Am. Chem. Soc. 2020, 142, 7443−7455
Read Online

ABSTRACT: Substituent effects play critical roles in both modulating reaction chemistry and supramolecular self-assembly processes. Using substituted terephthalate dianions (p-phthalic acid dianions; PTADAs), the effect of varying the type, number, and position of the substituents was explored in terms of their ability to regulate the inherent anion complexation features of a tetracationic macrocycle, cyclo[2](2,6-di(1H-imidazol-1-yl)pyridine)[2](1,4-dimethylenebenzene) (referred to as the Texas-sized molecular box, 1^{4+}), in the form of its tetrakis-PF_6^- salt in DMSO. Several of the tested substituents, including 2-OH, 2,5-di(OH), 2,5-di(NH_2), 2,5-di(Me), 2,5-di(Cl), 2,5-di(Br), and 2,5-di(I), were found to promote pseudorotaxane formation in contrast to what was seen for the parent PTADA system. Other derivatives of PTADA, including those with 2,3-di(OH), 2,6-di(OH), 2,5-di(OMe), 2,3,5,6-tetra(Cl), and 2,3,5,6-tetra(F) substituents, led only to so-called outside binding, where the anion interacts with 1^{4+} on the outside of the macrocyclic cavity. The differing binding modes produced by the choice of PTADA derivative were found to regulate further supramolecular self-assembly when the reaction components included additional metal cations (M). Depending on the specific choice of PTADA derivatives and metal cations (M = Co^{2+}, Ni^{2+}, Zn^{2+}, Cd^{2+}, Gd^{3+}, Nd^{3+}, Eu^{3+}, Sm^{3+}, Tb^{3+}), constructs involving one-dimensional polyrotaxanes, outside-type rotaxanated supramolecular organic frameworks (RSOFs), or three-dimensional metal−organic rotaxane frameworks (MORFs) could be stabilized. The presence and nature of the substituent were found to dictate which specific higher order self-assembled structure was obtained using a given metal. In the specific case of the 2,5-di(OH), 2,5-di(Cl), and 2,5-di(Br) PTADA derivatives and $^{3+}$Eu, so-called MORFs with distinct fluorescence emission properties could be produced. The present work serves to illustrate how small changes in guest substitution patterns may be used to control structure well beyond the first interaction sphere.

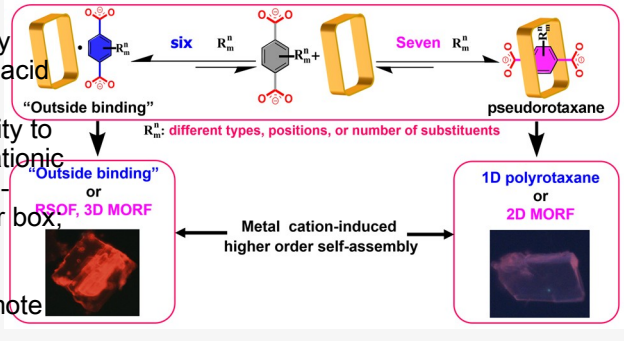

INTRODUCTION

Substituent effects are of significant interest to chemists and material scientists.[1,2] They also have a time-honored role in the context of supramolecular self-assembly. To date, changes in substituents have been used to modulate the structures of a number of key materials, including metal coordination cages,[3,4] supramolecular polymers,[5] metal−organic frameworks (MOFs),[6] and covalent organic frameworks (COFs).[7] Substituent effects have also been used to modulate the structures and properties of mechanically interlocked molecules (MIMs).[8] In the latter context, most prior effort has focused on the macrocycles or stopper moieties used to create catenanes or rotaxanes.[9] Few reports have considered the effect of substituents on the linear threading component (so-called axel); this is particularly true in the case of anionic hosts.[10] Here, we report a detailed study wherein 12 different substituted p-terephthalic acid dianions (PTADAs) were tested in conjunction with the so-called Texas-sized molecular box (cyclo[2]-(2,6-di(1H-imidazol-1-yl)pyridine)[2](1,4-dimethylenebenzene) (1^{4+}; studied as its tetrakis-PF_6^- salt). The resulting interactions were found to support a wide range of higher-order self-assembled multicomponent structures including: (1) those containing either interpenetrated or outside bound dianions, (2) pseudorotaxanes characterized by different interpenetration modes, and in conjunction with appropriately chosen cations both (3) metal−organic MIM species and (4) emissive MORFs, as shown in Scheme 1. In all cases, the nature of the substituent (H-bond donor, electron donating or withdrawing) was found

Received: December 14, 2019
Published: March 27, 2020

https://dx.doi.org/10.1021/jacs.9b13473
J. Am. Chem. Soc. 2020, 142, 7443−7455

Scheme 1. Effect of Substituents on p-Terephthalic Acid Dianions (PTADAs) in Stabilizing Different Supramolecular Constructs via Interaction with the Cationic Macrocycle 1^{4+}[a]

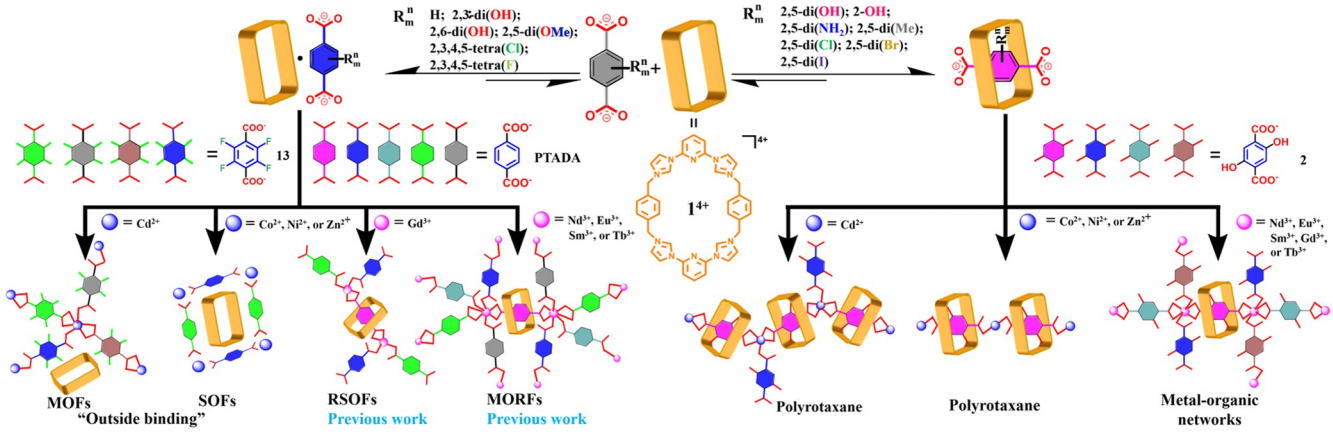

[a]Various colors are used to denote anions in different chemical environments.

to play a key, structure-defining role. Taken in concert, the present findings provide support for the notion that the choice of the anionic threading component can provide a means to guide and regulate the self- assembly of MIM-type structures derived from otherwise identical starting materials.

RESULTS AND DISCUSSION

Basic Interactions between 1^{4+} and PTADA Derivatives Bearing Different Substituents. As noted above, understanding the factors that can be used to regulate the nature of anion-based interpenetrated structures might allow novel MIMs and associated new materials to be created. In prior work, the p-terephthalic acid dianion (PTADA) was found to be effective as a linear threading component, allowing MIMs to be created from 1^{4+}.[11] However, these studies provided no insights into whether modifications to the PTADA structure could be used to control the nature of the products obtained from the basic PTADA + 1^{4+} self-assembly process. Therefore, we have now expanded the scope of dianionic substrates considered as possible threading components to include the 12 PTADA derivatives shown in Scheme 2.

Scheme 2. Structures of the Tetracationic Molecular Box Host (1^{4+}; Studied as Its Tetrakis-PF_6^- salt) and Dianionic PTADA-Derived Guests 2−13 (as their Tetramethylammonium (TMA$^+$) Salts) Considered in the Present Study

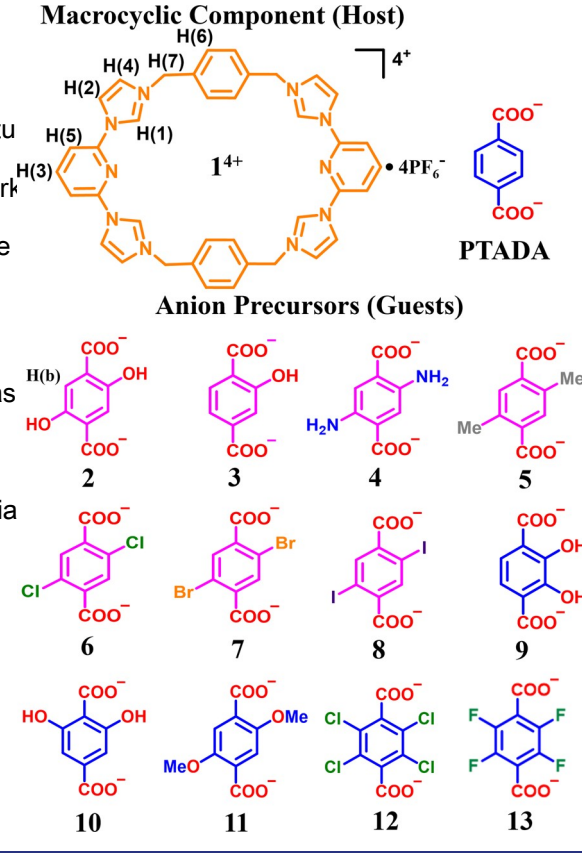

Interactions between 1^{4+} and Guests 2−12 in DMSO-d_6. As a first step toward exploring functionalized PTADAs as potential axels, we explored the interaction between 2,5-dihydroxyterephthalate dianion (2,5-di(OH)PTADA; 2) and 1^{4+}. (Note: all dianionic species considered in this study were obtained by adding 2 molar equiv of tetramethylammonium hydroxide ($TMA^+ \cdot OH^-$) to a DMSO-d_6 solution of the corresponding terephthalic acid derivative.) To obtain insights into the nature of the interactions between 1^{4+} and 2, changes in the ^{1}H NMR spectrum were monitored as 2 was added to 1^{4+}. (Note: all NMR spectroscopic experiments were performed in DMSO-d_6.) A Job plot analysis based on these spectral changes was then constructed (cf. Figure S1 in the Supporting Information). The resulting plot revealed that the value for y (defined as the product of chemical shift change for the signal corresponding to H(3) on 1^{4+} and the host concentration) reached a maximum value when the mole fraction was 0.5 ([H]/([H]+[G])), where [H] and [G] represent [host] and [guest], respectively). While it is subject to recognized caveats as a proof of stoichiometry,[12] such a finding is consistent with a 1:1 ([H]:[G]) interaction between 1^{4+} and anion 2 predominating in solution. Further support for this conclusion came from the fact that the chemical shift changes (most notably in the imidazole C−H resonance) observed when 1^{4+} (maintained at 0.50 mM) was titrated with increasing quantities of 2 fit well to a 1:1 binding model but less well to other simple stoichiometric alternatives. Assuming a 1:1 binding interaction allowed an association constant of $\log K_{assn} = 3.9(1)$ to be calculated (cf. Figures S2 and S3 in the Supporting Information).

https://dx.doi.org/10.1021/jacs.9b13473
J. Am.Chem. Soc. 2020, 142, 7443−7455

A mixture containing 1^{4+} and 1 molar equiv of 2 was then subject to a 2D diffusion ordered spectroscopic analysis (2D-DOSY). Similar diffusion times for the proton signals of 1^{4+} and 2 were found. Such a finding is interpreted in terms of 1 and 2 existing primarily in the form of a 1:1 complex, $2\subset1^{2+}$, under the conditions of analysis (cf. Figure S4 in the Supporting Information). A one-dimensional nuclear Overhauser enhancement (1D-NOE) spectroscopic analysis revealed cross peaks between H(b) on 2 and H(2,3,6) on 1^{4+}; this is as expected for a structure wherein 2 is inserted into the macrocyclic cavity of 1^{4+} to produce a pseudorotaxane-type structure as shown in Scheme 1 (cf. Figure S5 in the Supporting Information). This binding mode stands in contrast to what was seen for PTADA alone.[11d]

The interactions between the other PTADA derivatives considered in this study (i.e., 3−12) and 1^{4+} were investigated using similar solution-phase methods, namely ^{1}H NMR spectral titrations, Job plots, and 2D-DOSY and 1D-NOE spectroscopy. A binding model was considered for the host−guest interactions with 3:2 (G:H) stoichiometry, which mirrored that seen previously and included initial formation of two limiting complexes, namely those involving 1:1 and 1:2 ([H]:[G]) ratios, before further conversion to a 2:3 host−guest complex.[13] The binding stoichiometries, association constants (as log K_a) and binding modes inferred from these studies are summarized in Table 1 (cf. Figures S3, S8, S13, S18, S23, S28, S32, S36, S40, S44, and S48 in the Supporting Information).

Table 1. Summary of the Interactions between PTADA Derivatives 2−12 and 1^{4+} as Inferred from NMR Spectroscopic Analyses Carried Out in $DMSO_6$-d

guest	[H]:[G]	log K_a	mode[d]
PTADA	1:1[b]	3.5(1)	outside
2	1:1[b]	3.9(1)	insert[e]
3	2:3[c]	5.0(1),3.7(2),3.3(3)	insert[e]
4	2:3[c]	5.6(1),3.8(2),3.3(3)	insert[e]
5	1:1[b]	5.3(1)	insert[e]
6	1:1[b]	5.1(1)	insert[e]
7	1:1[b]	5.1(1)	insert[e]
8	1:1[b]	4.3(1)	insert[e]
9	1:1[b]	4.7(1)	outside
10	1:1[b]	4.0(1)	outside
11	1:1[b]	5.8(1)	outside
12	1:1[b]	4.9(1)	outside

[a]Equations governing the relevant equilibria are given in the following two footnotes. [b]$[H] + [G] \xrightarrow{K_{a1}} [HG]$. [c]$[H] + [G] \xrightarrow{K_{a1}} [HG]$, $[HG] + [G] \xrightarrow{K_{a2}} [HG_2]$, $[HG] + [HG_2] \xrightarrow{K_{a3}} [HG_3]$. [d]Mode inferred from 1D-NOE spectroscopic studies (cf. Figures S5, S10, S15, S20, S25, S29, and S33 in the Supporting Information). [e]"Insert" means the guest anion threads through the center of the host molecule to form a pseudorotaxane; see text for details.

There are two types of substituent(s) that can promote anion-forming ring-through structures. One type is embodied in anions 2−4, which contain hydrogen bond donor(s) ortho to the carboxylate unit(s). Within this set, the binding affinities corresponding to the first host−guest interaction event follow the order log $K_{a1}[1^{4+}\cdot4]$ > log $K_{a1}[1^{4+}\cdot3]$ > log $K_{a1}[1^{4+}\cdot2]$ (cf. Figures S3, S8, and S13 in the Supporting Information). Under identical conditions of ^{1}H NMR spectral analysis, the H(3) signal corresponding to the pyridine subunit of 1^{4+} was found to shift upfield to a greater extent for 4 > 3 > 2 (cf. Figure 1). These

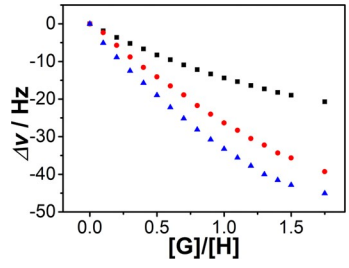

Figure 1. Chemical shift change values of H(3) (in 1^{4+}) as the [G]/[H] ratio is varied during the course of ^{1}H NMR spectroscopic titration experiments performed by adding 2, 3, 4 (G; labeled with black ■, red ●, and blue ▲, respectively) into a solution of $1^{4+}\cdot4PF_6^-$ (kept constant at 0.500 mM) (298 K; $DMSO_6$; 600 MHz).

findings are interpreted in terms of lone pair−π and π−π donor−acceptor interaction(s) playing a dominant role in the complexation. Explicit evidence for π−π donor−acceptor interactions came from the observation that treatment of 1^{4+} (1.00 mM in DMSO) with 1 molar equiv of dianions 2−4, as well as the other PTADA derivatives considered in this study, led to the observation of a presumed charge transfer (CT) band at longer wavelengths (cf. Figure S49 in the Supporting Information).

The other PTADA substituent class found to stabilize an inserted binding mode is represented by 5−8. These four guests lack substituents capable of supporting intramolecular hydrogen bond interactions. Relatively strong 1:1 binding affinities on the order of log $K_{a1}[1^{4+}\cdot5]$ > log $K_{a1}[1^{4+}\cdot6]$ ≈ log $K_{a1}[1^{4+}\cdot7]$ > log $K_{a1}[1^{4+}\cdot8]$ were deduced from the associated ^{1}H NMR spectral titrations. In the case of 5, the addition of ≤1 molar equiv of the dianionic guest to 1^{4+} leads to a broadening and then disappearance of the signal corresponding to proton H(1) on the macrocyclic host (cf. Figure S17 in the Supporting Information). This finding is taken as evidence that the complexation between 5 and 1^{4+} is dynamic and occurs on the NMR time scale. In contrast, only one set of proton signals is observed when analogous titrations are carried out with 6, 7, or 8, a finding interpreted in terms of fast exchange between the bound and unbound forms (i.e., $1^{4+}\cdot$anion] and free 1^{4+} + anion) at room temperature. It is to be noted that adding near or less than 1 molar equiv of these dianionic guests induces a downfield shift in the H(1) resonance of 1^{4+} as follows: 6 > 7 > 8 (cf. Figure 2a). Meanwhile, the upfield chemical shift change for the H(3) resonance decreases with increasing guest con-

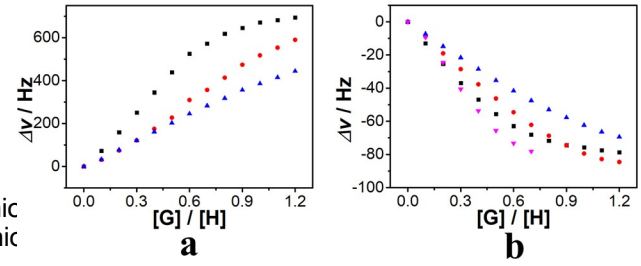

Figure 2. Chemical shift change values seen for the H(1) (a) and H(3) (b) resonances of $1^{4+}\cdot4PF_6^-$ (maintained at 0.500 mM) as a function of increasing [G]/[H] (G = 5, 6, 7, or 8, labeled with magenta ▲, black ■, red ●, and blue ▼, respectively, and H^+) as measured via ^{1}H NMR spectral titrations carried out under otherwise identical experimental conditions (298 K; $DMSO_6$; 600 MHz). Note: in the case of 1^{4+} and 5, precipitation occurred when the [G]/[H] ratio exceeded 0.8.

https://dx.doi.org/10.1021/jacs.9b13473
J. Am.Chem. Soc. 2020, 142, 7443−7455

tration in the order 5 > 6 ≈ 7 > 8 (cf. Figure 2b), as do the calculated 1:1 log K_a values. These results are interpreted in terms of a balance between (1) steric effects, which would le the carboxylate anions to adopt a more orthogonal orientatio relative to the phenyl core, and (2) electronic effects, which would affect the charge density on the anion. Nevertheless, i important to note that substituents as large as bromine may tolerated at the 2- and 5-positions of the PTADA core withou triggering an appreciable reduction in the anion binding affini

1D-NOE spectral analyses of 1:1 mixtures of the 2,3- and dihydroxy PTADA derivatives 9 and 10, respectively, and 1^{4+} revealed no discernible correlation-ascribable signals in eith case. The same was true for the 2,5-dimethoxy and tetrachlor derivatives 11 and 12, respectively. This was taken as evidence that these latter anions bind 1^{4+} via a so-called outside binding mode, as was found initially in the case of the unsubstituted parent, PTADA.[11d]

Further evidence that anions 2−12 would associate with 1^{4+} came from electrospray ionization high-resolution mass spectrometric (ESI-HRMS) analyses. For instance, ESI-HRMS analyses of complexes containing 1^{4+} and 2 revealed a peak corresponding to $[1^{4+} + 2\text{-H}]^{\cdot+}$ (m/z 825.2879; calcd m/z 825.2898) (cf. Table S1 in the Supporting Information). Analogous samples derived from the other tested anionic guests (i.e., 3−12) were also obtained and analyzed. Again, evidence of complex formation was seen in all cases (cf. Figures S50−S6 the Supporting Information).

Interactions between 1^{4+} and Guests 2−12 in the Solid State. In order to obtain additional insights into the likely binding modes for the complexes formed from 1^{4+} and the various anionic guests 2−12, an effort was made to obtain diffraction-grade crystals of the adducts $[1^{4+}\cdot n^{2+}]$ (n = 2−12). As initially inferred from the 1D-NOE studies (vide supra), the resulting structures revealed that guests 2−8 thread through t cavity of 1^{4+} to give pseudorotaxane-type complexes. However the specifics were found to vary according to the class of PT derivative employed.

The intramolecular hydrogen bonds in 2−4 invoked to rationalize the solution-phase binding behavior were seen in t solid-state structures of complexes $2_2\cdot 12DMF\cdot 6H_2O$, $(2H^+\cdot 1^{4+})\cdot 3\cdot(H^+\cdot 3)_4\cdot 4H_2O$, and $1^{4+}\cdot 4_2\cdot 16H_2O$. Here, the host adopts a "boxlike" conformation. The carboxylate anion in these three bound guests was found to be relatively coplanar with the benzene ring. Presumably, this favors π−π donor−acceptor interactions with 1^{4+} and accounts in part for the observed insert binding mode. Consistent with this supposition are the relatively short separations (around 3.3 Å) seen between the benzene rings in 2−4 and the nitrogen atoms on the pyridine rings of 1^{4+} in the case of complexes $2_2\cdot 2DMF\cdot 6H_2O$, $(2H^+\cdot 1^{4+})\cdot 3\cdot(H^+\cdot 3)_4\cdot 4H_2O$, and $1^{4+}\cdot 4_2\cdot 16H_2O$ (cf. Figure 3c). Short distances (≤3.25 Å) between the oxygen atom of the −OH moieties and the nitrogen atom of the $-NH_2$ substituent on 2−4 and the bridging benzene rings on 1^{4+} were also seen.

Another insert binding mode was found in the complexes formed from 5−8 as inferred from the single-crystal structures of $1^{4+}\cdot 5_2\cdot 14H_2O$, $1^{4+}\cdot 6_2\cdot 12H_2O$, $1^{4+}\cdot 7_2\cdot 10H_2O$, and $1^{4+}\cdot 8_2\cdot 10H_2O\cdot CH_3CN$ (cf. Figure 4). It is noteworthy that 1^{4+} adopts a "chair" conformation in these complexes; this stands in contrast with the "box" mode seen in the above studies. Nevertheless, the carboxylate moieties are again essentially orthogonal to the linking benzene ring. This results in an opening up of the structures and formation of pseudorotaxanes where the central phenyl of the anionic guests is perpendicular to the benzene plane on the macrocycle 1^{4+}. The shortest distance between the C atom of the CH_3 substituent on 5, or the Cl, Br, or I atoms on 6−8, to the two pyridine rings of 1^{4+} is around 3.5 Å, while the distance between the benzene ring on the guest and the pyridine ring on 1^{4+} is ca. 3.0 Å (cf. Figure 4).

Consistent with what was inferred from the solution studies discussed above, guests 9−12 all interact with 1^{4+} via outside binding modes in the solid state, as determined via single-crystal X-ray diffraction analyses (cf. Figure 5). This mirrors what was seen in the case of 1^{4+} and the parent PTADA guest, the structure of which ($1^{4+}\cdot PTADA_2\cdot 16H_2O$) is also shown in Figure 5 for comparison.[11d] Presumably, a combination of attractive π−π donor−acceptor, hydrogen-bond, and electro-

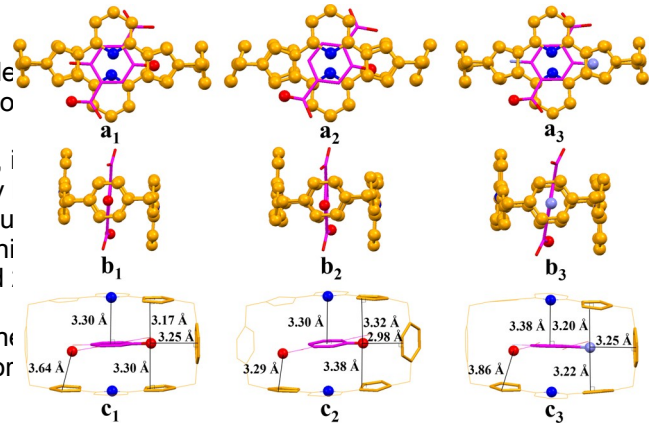

Figure 3. Top (a_1−a_3), side (b_1−b_3), and front (c_1−c_3) views of the solid-state structures of $1^{4+}\cdot 2_2\cdot 2DMF\cdot 6H_2O$, $(2H^+\cdot 1^{4+})\cdot 3\cdot(H^+\cdot 3)_4\cdot 4H_2O$ and $1^{4+}\cdot 4_2\cdot 16H_2O$, respectively, highlighting key distances and the overall "box" conformations of 1^{4+} seen in these three complexes. Selected key distances are shown to aid in visualization, as is the "box" conformation of 1^{4+} in outline form. The red, blue, and light blue balls represent selected carboxylate O, host pyridine N, and guest (4) amino N atoms, respectively. Some or all of the counteranions, solvent molecules, and hydrogen atoms have been omitted for clarity.

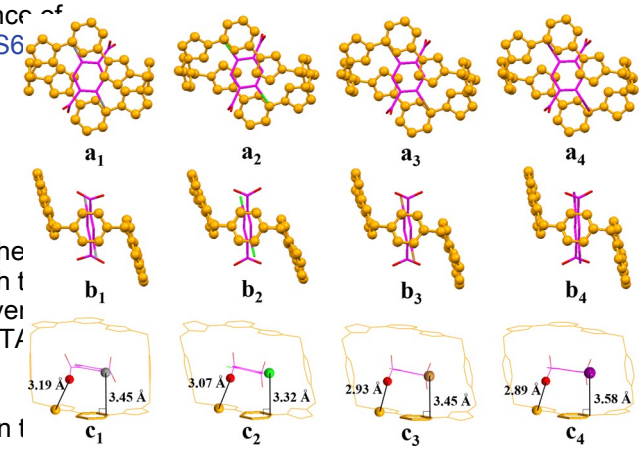

Figure 4. Top (a_1−a_4), side (b_1−b_4), and front (c_1−c_4) views of the single-crystal structures of $1^{4+}\cdot 5_2\cdot 14H_2O$, $1^{4+}\cdot 6_2\cdot 12H_2O$, $1^{4+}\cdot 7_2\cdot 10H_2O$, and $1^{4+}\cdot 8_2\cdot 10H_2O\cdot CH_3CN$, respectively, highlighting some key distances and the "twist chair" conformation of 1^{4+} seen in these complexes. Selected key distances are shown to aid in visualization, as is the "twist chair" conformation of 1^{4+} in outline form. The red, gray, green, brown, and purple balls represent selected carbonyl C, Cl, Br, and I atoms on the threading anions 5−8, respectively. Some or all of the counteranions, solvent molecules, and hydrogen atoms have been omitted for clarity.

https://dx.doi.org/10.1021/jacs.9b13473
J. Am. Chem. Soc. 2020, 142, 7443−7455

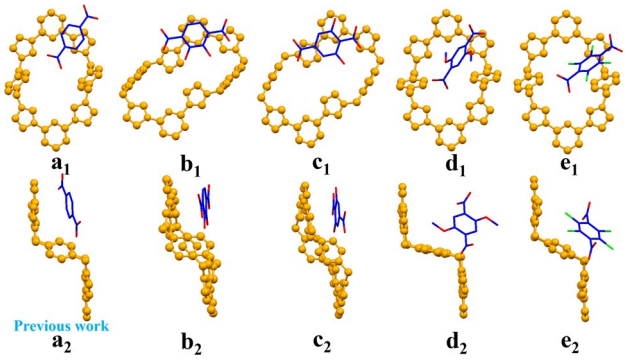

Figure 5. Top (a_1−e_1) and side (a_2−e_2) views of the "twist chair" conformation of 1^{4+} with the guest PTADA, 9, 10, 11, or 12 as seen in the single crystal structures of $PTADA_2 \cdot 16H_2O$ (a), $1^{4+} \cdot 9_2 \cdot 14H_2O$ (b), $1^{4+} \cdot 10_2 \cdot 12H_2O$ (c), $1^{4+} \cdot 11_2 \cdot 7H_2O$ (d), $1^{4+} \cdot 12_2 \cdot DMF \cdot 7H_2O$ (e), respectively. Some or all of the counteranions, solvent molecules, and hydrogen atoms have been omitted for clarity.

static interactions serve to stabilize the observed extracavity binding, while presumably unfavorable steric effects militate against pseudorotaxane formation (cf. Figure 5 and Figures S70−S73 in the Supporting Information). As detailed below, an effort was made to gain greater insight into the relative importance of these various putative influences.

On the basis of the above results, we conclude that when the size of the substituent lies between those of −H and −OMe and the PTADA core is monosubstituted or para-disubstituted, pseudorotaxane complexes with 1^{4+} are stabilized. Unsubstituted, ortho- or meta-disubstituted, and more sterically hindered versions of PTADA tend to bind outside of macrocycle 1^{4+}. The type of structure formed with PTADA-type substrates can thus now be predicted with some degree of confidence.

Interactions between 1^{4+} and Guests 2−13 as Probed Using Calculations. Theoretical calculations were carried out in an effort to obtain additional insight into the interactions between 1^{4+} and each anionic precursor (i.e., PTADA or anions 2−13). Using the single-crystal structures reported in this study as the starting point, 37 outside and 4 interpenetrated binding modes (cf. Table S5 in the Supporting Information) involving 1^{4+} and these anions were considered using the molecular mechanics (MM+) force field and semiempirical methods (PM3) included in the HyperChem 7.5 program. Both vacuum and aqueous solutions (concentrations of 0.1 M in each component) were considered in these calculations. The most stable outside and insert modes for each host−guest complex were then compared. The energy difference between these two limiting binding modes was considered to reflect the thermodynamic propensity of any given pair to stabilize a pseudorotaxane structure, as opposed to one involving only an outside interaction (cf. Figure 6 and the Supporting Information).

The calculation results lead us to suggest that the anionic substrates PTADA, 2−4, 9, and 10 will adopt the inset mode, In1, when they thread through the cavity of 1^{4+}. This calculation-based finding is consistent with the pseudorotaxane structures $[1^{4+} \cdot n]$ (n = 2−4) seen in the single-crystal X-ray diffraction structures of $1^{4+} \cdot 2_2 \cdot 2DMF \cdot 6H_2O$, $(2H^+ \cdot 1^{4+}) \cdot 3 \cdot (H^+ \cdot 3)_4 \cdot 4H_2O$, and $1^{4+} \cdot 4_2 \cdot 16H_2O$. In contrast, guests 5−8 and 11−13 insert into 1^{4+} via a second mode, In2, as represented by the interpenetrated structures seen for $[1^{4+} \cdot n]$ (n = 5−8) in single-crystal structures of $1^{4+} \cdot 5_2 \cdot 14H_2O$, $1^{4+} \cdot 6_2 \cdot 12H_2O$, $1^{4+} \cdot 7_2 \cdot 10H_2O$, and $1^{4+} \cdot 8_2 \cdot 10H_2O \cdot CH_3CN$. An outside binding mode, Out1, was found to be preferred in the case of PTADA, 2−4, 9, and 10. Mode Out2 is possible for anions 5−8 and 11−13. It is noteworthy that all the tested anion precursors adopt two stable conformations. In one mode, the carboxylate moiety is coplanar with the central benzene ring (e.g., PTADA, 2−4, 9, and 10). All of these anions favor either the In1 or Out1 binding modes when they are allowed to interact with 1^{4+}. Another mode is seen in the case of anions 5−8 and 11−13. Here, the carboxylate subunits are perpendicular to the benzene plane. These anions interact with 1^{4+} preferably through the In2 or Out2 modes.

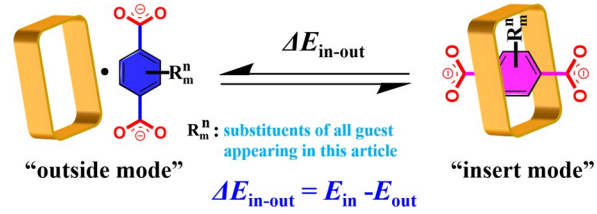

Figure 6. Chemical pseudoequilibrium between limiting external ("outside) and internal ("insert") binding modes.

The ΔE_{in-out} values summarized in Table 2 provide support for the notion that the inset mode is more stable than outside binding in all cases under vacuum. However, solution effects play an important role in defining the complexation mode. Specifically, we have found through these calculations that in water pseudorotaxane formation is favored in the case of 2−8. However, outside binding is still seen in the complexes containing PTADA and 9−13.

The above findings, considered in concert, provide support for the notion that the substituents on the anion not only change the electronic and steric features of what are ostensibly similar substrates but can also induce changes in the conformation of the carboxylate moieties (i.e., $-CO_2^-$ moieties that are coplanar vs perpendicular to the linking benzene ring). This latter change appears to have a large effect on whether an insert or outside binding mode is favored. The substituents on the anion skeleton appear to affect the relative stability of the outside and inside modes. In other words, we suggest that the experimentally determined differences reflect thermodynamic rather than kinetic control.

Effect of Anionic Substituents on the Higher-Order Self-Assembly of 1^{4+} and Metal Cations (M). Multicomponent Self-Assembly. Comparison among PTADA or 2, 1^{4+}, and M (M = Co^{2+}, Ni^{2+}, Zn^{2+}). The fact that different binding modes with 1^{4+} could be stabilized via the choice of substituent on the PTADA core led us to explore how, if, these initial structural differences might translate into control over the preparation of higher order self-assembled species. In an initial set of studies, 1^{4+} (2.0 mM), 2 (6.0 mM), and M (M = Co^{2+}, Ni^{2+}, Zn^{2+}; 12.0 mM as their NO_3^- salts) were mixed in $DMF/CH_3CN/H_2O$ (1/1/1, v/v/v) and allowed to stand uncapped for 3 days to 2 weeks. This "one-pot" procedure yielded diffraction-grade crystals of $[1^{4+} \cdot 2_3 \cdot Co^{2+} \cdot 4H_2O] \cdot 18H_2O$, $[1^{4+} \cdot 2_3 \cdot Ni^{2+} \cdot 4H_2O] \cdot 2DMF \cdot 7H_2O$, and $[1^{4+} \cdot 2_3 \cdot Zn^{2+} \cdot 4H_2O] \cdot 13H_2O$.

Single-crystal X-ray diffraction analyses revealed the formation of 1D metal−organic polyrotaxanes, $[1^{4+} \cdot 2 \cdot M]_n$ (M = Co^{2+}, Ni^{2+}, Zn^{2+}), in all three cases (cf. Figure 7b). In these structures, the anionic guest 2 inserts into 1^{4+} to provide a formal pseudorotaxane subunit. Cation coordination by a pair of carboxyl groups from neighboring pseudorotaxane subunits

https://dx.doi.org/10.1021/jacs.9b13473
J. Am. Chem. Soc. 2020, 142, 7443−7455

Table 2. Pictorial Representations of the Lowest Energy External and Internal Binding Modes and the Difference between the Minimum Internal Binding Energy (E_{in}) and the Minimum External Binding Energy (E_{out}) as Calculated under Vacuum and in Water using HyperChem7.5

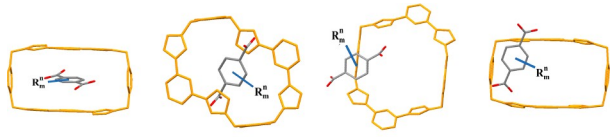

G	most stable insert complex	most stable outside binding	$\Delta E_{in-out} = E_{in} - E_{out}$ (kcal/mol)[a]			
			method A[b]	method B[b]	method C[b]	method D[b]
PTADA	In1	Out1	−11.88	7.86	10.74	41.53
2	In1	Out1	−11.23	1.3	−3.94	−6.92
3	In1	Out1	−13.4	1.36	−12.95	−2.79
4	In1	Out1	−13.95	0.33	−1.26	−12.88
5	In2	Out2	−10.53	−8.64	−9.34	−12.07
6	In2	Out2	−10.36	−6.48	−11.53	−10.56
7	In2	Out2	−10.31	−6.68	2.68	−28.99
8	In2	Out2	−11.12	−5.57	8.39	−27.96
9	In1	Out1	−12.99	1.01	2.7	7.08
10	In1	Out1	−12.96	−0.45	26.07	245.9
11	In2	Out2	−6.84	−11.19	15.94	5.03
12	In2	Out2	−5.54	10.58	63.55	53.40
13	In2	Out2	−6.16	3.28	84.53	6.67

[a] E_{in} and E_{out} are the respective atomic reaction formation energies. ΔE_{in-out} is the enthalpy change from the "outside" binding mode structure, considered as the initial state, to the insert binding mode structure taken as the final state. [b] A, B, C, and D represent respectively four simulation approaches: molecular mechanics (MM+) force field under vacuum, semiempirical methods (PM3) under vacuum, molecular mechanics (MM+) force field in water, and semiempirical methods (PM3) in water. Solvation was accounted for by applying a 2.55 nm × 2.55 nm × 2.55 nm periodic box.

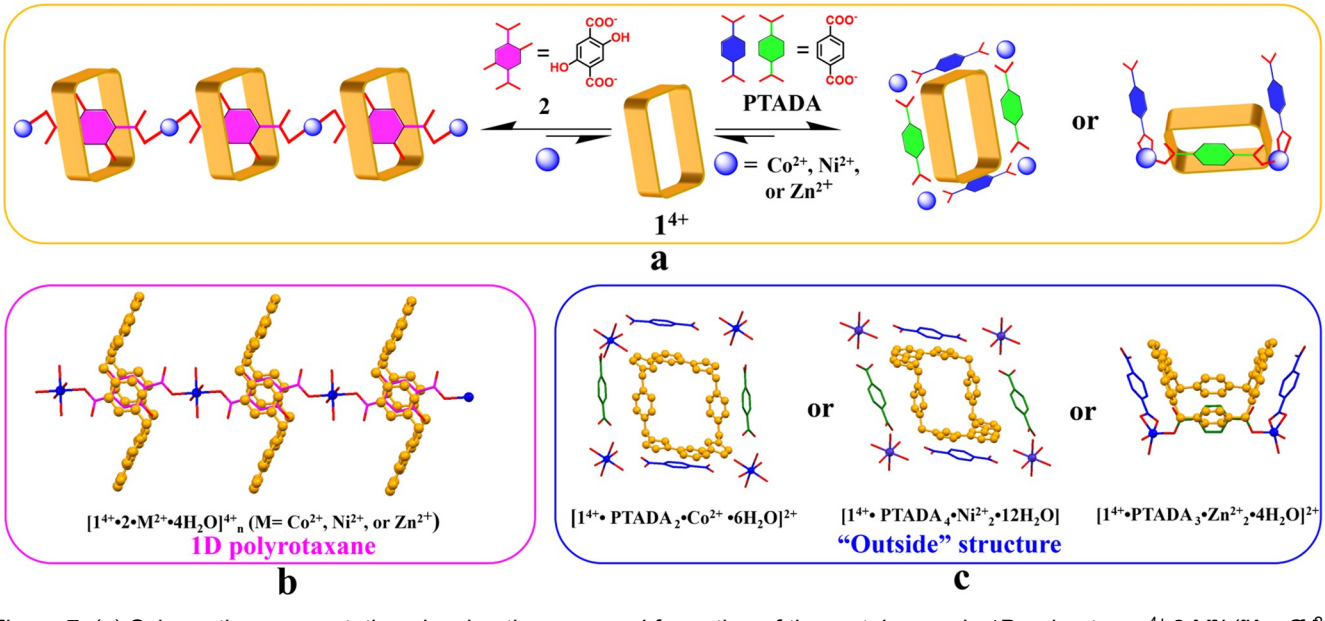

Figure 7. (a) Schematic representation showing the proposed formation of the metal−organic 1D polyrotaxane complexes (M = Co^{2+}, Ni^{2+}, Zn^{2+}) and outside binding structure of the complexes formed with 1^{4+}, 1M, and PTADA. (b) Top view of single-crystal structures of 1D polyrotaxanes $[1^{4+}\cdot 2\cdot M]_n$ (M = Co^{2+}, Ni^{2+}, Zn^{2+}). (c) Separate structure without MIMs formed among 1^{4+}, PTADA, and Co^{2+}, Ni^{2+}, or Zn^{2+} as determined via single-crystal structural analysis of $[1^{4+}\cdot PTADA_3\cdot Co^{2+}\cdot 6H_2O]\cdot 2DMF\cdot 2H_2O$, $[1^{4+}\cdot PTADA_4\cdot Ni^{2+}_2\cdot 6H_2O]\cdot 34H_2O$, and $[1^{4+}_2\cdot PTADA_9\cdot Zn^{2+}_6\cdot 12H_2O]\cdot 2OH^-\cdot 88.5H_2O$. All metal atoms are highlighted as blue balls. Different colors are used for the anions to illustrate the different local chemical environments. Some or all of the counteranions, solvent molecules, and hydrogen atoms have been omitted for clarity.

then serves to produce the observed 1D polyrotaxane necklace-like structures (cf. Figure 7c). In contrast to what was seen in the metal-free pseudorotaxane formed from 1^{4+} and 2 (i.e., $1^{4+}\cdot 2_2\cdot 2DMF\cdot 6H_2O$), where the benzene ring on 2 is orthogonal to the benzene ring of 1^{4+}, in these three cation-containing polyrotaxanes the benzene ring on 2 is parallel to the benzene ring of 1^{4+}. Of note is that formation of the carboxylate−cation coordination bonds serves to weaken the intramolecular hydrogen bonds between the substituent (−OH) and the carboxylate anion, which frees up the hydroxyl groups to form hydrogen bonds with the imidazole C−H protons present in 1^{4+}

https://dx.doi.org/10.1021/jacs.9b13473
J. Am.Chem. Soc. 2020, 142, 7443−7455

(cf. Figure 7b). Presumably, these ancillary interactions add stability to the overall complex.

In order to assess the effect of the −OH substituents present in 2, analogous studies were carried out using the parent PTADA system. However, in contrast to what was seen for $[1^{4+}2\cdot M]_n$ (M = Co^{2+}, Ni^{2+}, Zn^{2+}), these crystallization efforts yielded only discrete structures consisting of $[1^{4+}\cdot PTADA_3\cdot Co^{2+}\cdot 6H_2O]\cdot 2DMF\cdot 2H_2O$, $[1^{4+}\cdot PTADA_4\cdot Ni^{2+}_2\cdot 6H_2O]\cdot 34H_2O$, and $[1^{4+}_2\cdot PTADA_9\cdot Zn^{2+}_6\cdot 12H_2O]\cdot 2OH^-\cdot 88.5H_2O$. Specifically, various arrangements of dianions and hydrated metal cations are seen to reside outside the core of 1^{4+} (cf. Figure 7c). Presumably, this reflects the fact that PTADA per se is ineffective at stabilizing an insert-type pseudorotaxane structure. The difference between the structures formed with 2 and with PTADA provided us with a preliminary indication that, in systems involving complexation with 1^{4+}, small changes in guest structure can serve to control structure well beyond the first coordination sphere.

Complexation between PTADA or 2 and Co^{2+} was considered in the context of the pseudoequilibrium shown in Scheme 3. A MM+ force field calculations was carried out under vacuum and in aqueous solution (0.1 M for each component). The results obtained proved to be consistent with the inference that, in comparison with PTADA, 2 is a better ligand for M (M = Co^{2+}, Ni^{2+}, Zn^{2+}) (cf. Table 3 and Table S12 the Supporting Information).

Scheme 3. Complexation Process between M (M^{2+} = Co^{2+}, Zn^{2+}) and PTADA or 2 Shown in the Form of a Chemical Equilibrium[a]

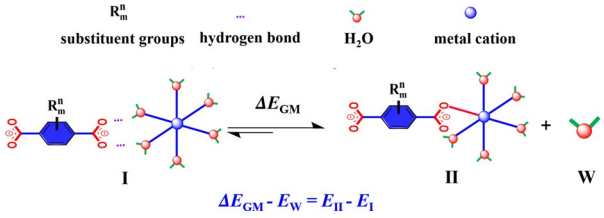

[a]E_I, E_{II}, and E_W are their atomic reaction formation energies. ΔE_{GM} is the enthalpy change from complex I as the initial state to complex II as the final state.

Moreover, three-component self-assembly $1^{4+}\cdot 2_3\cdot [M\cdot 5H_2O]$ (M = Co^{2+}, Ni^{2+}, Zn^{2+}), was considered in the reaction between an inserted anion and $M(H_2O)_6$. The resulting calculation-derived results provide support for the conclusion that 2 is more efficient in stabilizing species such as $1^{4+}\cdot 2_3\cdot M\cdot 5H_2O]$ (M = Co^{2+}, Ni^{2+}, Zn^{2+}) (cf. Scheme 4 , Table 4, and Tables S11−S12 in the Supporting Information).

Table 3. Energy Difference (kcal/mol) between the Metal Complex and Hydrogen Bond Induced Complex (Structures on the Right and Left of Scheme 3, Respectively) Calculated under Vacuum and Water Solution Conditions using Hyperchem 7.5

		$\Delta E_{GM} - \Delta E_W$ (kcal/mol)		
method[a]	anion	Co^{2+}	Ni^{2+}	Zn^{2+}
A	PTADA	0.71	0.68	0.93
	2	−0.21	−0.01	0.16
C	PTADA	7.38	−4.92	−2.58
	2	−4.01	−14.55	−12.24

[a]A and C represent respectively different simulation approaches: molecular mechanics (MM+) under vacuum and in water. Solvation is accounted for by applying a 2.55 nm × 2.55 nm × 2.55 nm periodic box.

Scheme 4. Possible Interactions among 1^{4+}, M (M = Co^{2+}, Ni^{2+}, Zn^{2+}), and PTADA or 2 Shown in the Form of a Chemical Equilibrium[a]

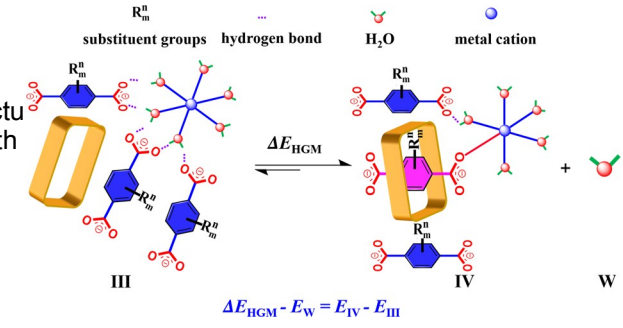

[a]E_{III}, E_{IV}, and E_W are the formation energies. ΔE_{HGM} is the enthalpy change from the ternary complex III as the initial state to the ternary complex IV as the final state.

Table 4. Energy Difference (kcal/mol) between the Metal Complex and Hydrogen Bond Induced Complex (Structures on the Right and Left of Scheme 4, Respectively) Calculated under Vacuum and Water Solution Conditions Using Hyperchem 7.5

		$\Delta E_{HGM} - \Delta E_W$ (kcal/mol)		
method[a]	anion	Co^{2+}	Ni^{2+}	Zn^{2+}
A	PTADA	−10.15	−5.92	−6.64
	2	−11.52	−11.53	−11.27
C	PTADA	20.94	20.91	33.80
	2	−17.64	−29.75	−33.17

[a]A and C represent respectively different simulation approaches involving the molecular mechanics (MM+) force field applied under vacuum and in water. Solvation is accounted for by applying a 2.55 nm × 2.55 nm × 2.55 nm periodic box.

In comparison with PTADA, dianion 2 is better able to form metal complexes (a presumed thermodynamic effect) and thus promote multicomponent self-assembly, a conclusion supported by both experimental findings and theory. To the extent such a supposition is correct, it provides further support for the notion that the substituent(s) on the anion affect not only initial supramolecular complex formation but also the ensuing metal-based self-assembly.

Multicomponent Self-Assembly Comparison among PTADA or 2, 1^{4+}, and Cd^{2+}. An effort was then made to explore the effect of larger metal cations on the basic self-assembly procedure. In the specific case of Cd^{2+} diffraction-grade crystals of what proved to be self-assembled multi-component structures could be obtained by mixing $Cd(NO_3)_2\cdot 4H_2O$ and 1^{4+} with either 2 or 13 in DMF/H_2O (1/1, v/v). In contrast, only metal-free constructs containing 1^{4+} and the dianions in question were found for 9−12. The MOF structure containing PTADA and Cd^{2+} was obtained in the absence of 1^{4+}. An analysis of single crystals of $[1^{4+}\cdot 2_3\cdot Cd^{2+}\cdot 2H_2O]\cdot 12H_2O\cdot DMF$ revealed a 1D polyrotaxane structure (Figure 8). In contrast, 13 (i.e., 2,3,5,6-tetra(F)PTADA) was found to stabilize an anionic MOF wherein both the anion-coordinated

https://dx.doi.org/10.1021/jacs.9b13473
J. Am.Chem. Soc. 2020, 142, 7443−7455

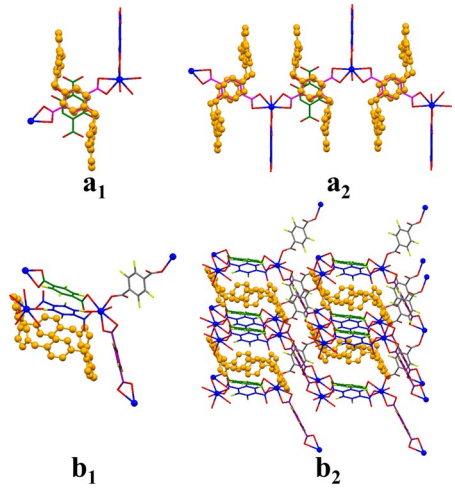

Figure 8. Top view of the basic unit (a1) and truncated view of the polyrotaxane (a2) found in the structure of $[1^{4+}\cdot 2_3\cdot Cd^{2+}\cdot 2H_2O]\cdot 12H_2O\cdot DMF$. Also shown is the anionic unit (b1) present in the MOF produced from 13, Cd^{2+}, and 1^{4+} and (b2) a partial view of the more extended structure comprising $[1^{4+}\cdot 13_4\cdot Cd^{2+}\cdot 2H_2O]\cdot DMF$.

metal complex (i.e., $13\cdot Cd^{2+}\cdot 2H_2O$) and the tetracationic box 1^{4+} are located in the cavity. Thus, even though self-assembly occurs, no interpenetrated structure was obtained. The contrast between what was seen with 2 and 13 (and other anions tested) lends further support to the notion that substituent effects can play a key role in regulating the self-assembly of ostensibly similar molecular- and atomic-scale building blocks.

Comparison of the Multicomponent Self-Assembly Achieved Using PTADA or 2, 1^{4+}, and Lanthanide Metal Cations M ($M = Tb^{3+}$, Gd^{3+}, Sm^{3+}, Tb^{3+}, Nd^{3+}). As a complement to the above studies, efforts were made to explore the extended structures if any, stabilized by the lanthanide metal cations. Cations of the lanthanide series are generally considered to be relatively hard Lewis acids and have been recognized for their all-important roles in catalysis and optical materials.[14] In previous work, PTADA was found capable of supporting a rotaxanated supramolecular organic framework (RSOF), $[1^{4+}\cdot PTADA_5\cdot Gd^{3+}_2\cdot 8H_2O]_n$, when it was cocrystallized with Gd^{3+} in the presence of 1^{4+} (cf. Figure 9c).[11a] To test the effect of replacing PTADA by 2, an analogous crystal growth procedure was employed. Specifically, 2 molar equiv of gadolinium nitrate hydrate ($Gd(NO_3)_3\cdot 6H_2O$) was dissolved in a glass vial containing 0.1 mL of water. Then, 1 molar equiv of 1^{4+} (2 mM) was added. Finally, a 5 molar equiv solution of 2 in DMF/H_2O (1/1, v/v) was layered slowly with a DMF/H_2O mixture of (1/1, v/v). After the mixture was allowed to stand for 2 weeks, diffraction-grade single-crystal samples of $[1^{4+}\cdot 2_5\cdot Gd^{3+}_2\cdot 6H_2O]\cdot H_2O\cdot 4DMF$ were obtained.

In the case of the previously reported RSOF formed with PTADA, 1^{4+}, and Gd^{3+}, the rotaxane units are connected by intermolecular hydrogen bonds.[11a] In marked contrast, the RSOF produced with 2, namely $[1^{4+}\cdot 2_5\cdot Gd^{3+}_2\cdot 6H_2O]_n$, consists of a more complex 2D layered metal−organic rotaxane framework (2D MORF). In this MORF, dianion 2 is threaded through the cavity of 1^{4+} in a manner analogous to what was seen in the 1D polyrotaxanes $[1^{4+}\cdot 2\cdot M]_n$ ($M = Co^{2+}$, Ni^{2+}, Zn^{2+}) discussed above. The rotaxane repeating units are connected via coordination bonds. This creates a rotaxaned network wherein the individual network layers are further connected by apparent hydrogen-bonding interactions to give the final structure (cf. Figure 9b).

To explore whether the structural differences caused by formally replacing PTADA with 2 would be recapitulated in the case of other trivalent lanthanide cations, similar multi-component "one-pot" self-assembly procedures with 2, 1^{4+}, and M ($M = Nd^{3+}$, Sm^{3+}, Eu^{3+}, Tb^{3+}) were carried out (Table 5). In contrast to the 3D MORFs obtained in the case of prior

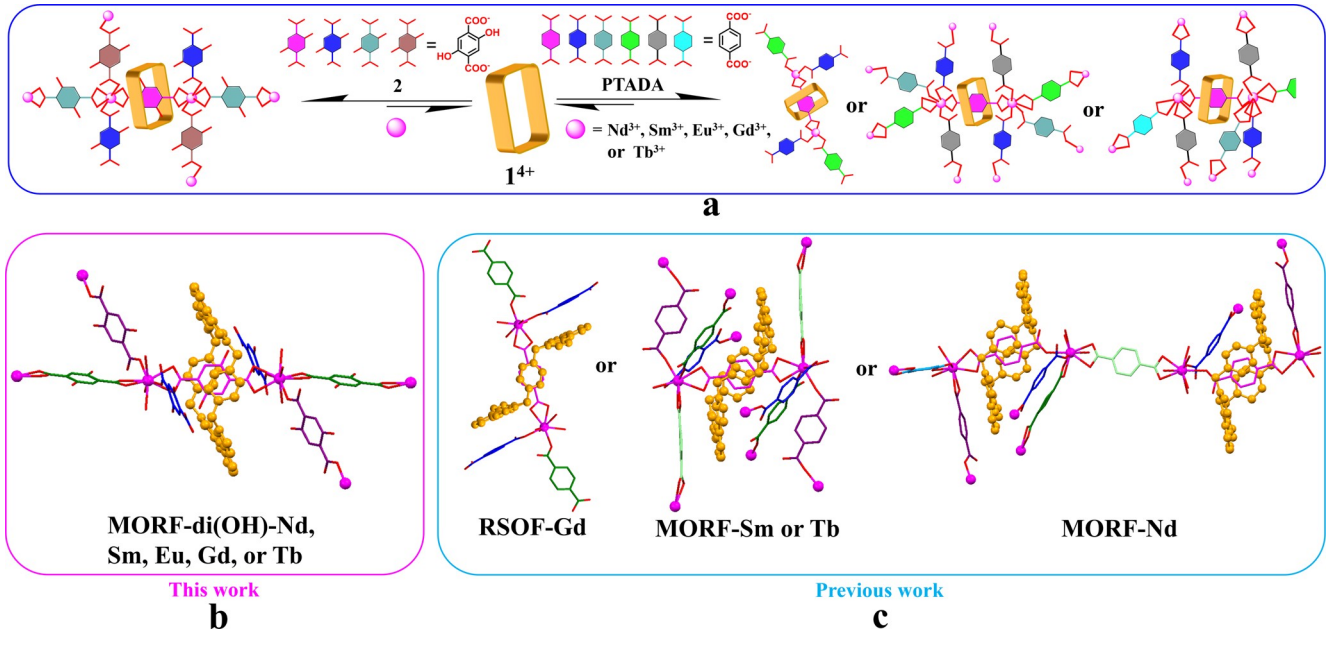

Figure 9. (a) Schematic representation showing the proposed formation of the 2D MORFs containing $[1^{4+}\cdot 2_n\cdot M]_n$ ($M = Nd^{3+}$, Sm^{3+}, Eu^{3+}, Gd^{3+}, or Tb^{3+}) and rotaxane or 3D MORF structures formed from 1^{4+}, M, and PTADA or 2. (b) 2D MORF structures formed from 1^{4+}, M ($M = Nd^{3+}$, Sm^{3+}, Eu^{3+}, Gd^{3+}, or Tb^{3+}), and 2. (c) RSOF or 3D MORF structure formed from 1^{4+}, M ($M = Gd^{3+}$, Sm^{3+}, Tb^{3+}, Nd^{3+}), and PTADA. All metal atoms are shown as blue balls. Colors are used to highlight the different local chemical environments of the various linking anions.

https://dx.doi.org/10.1021/jacs.9b13473
J. Am. Chem. Soc. 2020, 142, 7443−7455

Table 5. Summary of Guest (PTADA or 2), 1, and M Three-Component Self-Assembled Structures

	anionic precursor			
	PTADA		2	
metal	mode	type	mode	type
Co^{2+} Ni^{2+} Zn^{2+}	outside		inside	polyrotaxane
Gd^{3+}	inside	RSOFs	inside	MORFs
Nd^{3+} Sm^{3+} Eu^{3+} Tb^{3+}	inside	3D MORFs	inside	MORFs

studies involving PTADA (cf. Figure 9b),[14b] the introduction of hydroxyl substituents on the 2 - and 5-positions of the PTADA core (i.e., to produce 2) gave rise to similar 2D MORFs, namely, $[1^{4+}\cdot 2_5\cdot M_2\cdot 6H_2O]\cdot 4H_2O\cdot 4DMF$ (M = Nd^{3+}, Sm^{3+}, Eu^{3+}, Tb^{3+}), in the case of all four test cations. These 2D MORFs are essentially identical with the structure formed via the self-assembly of Gd^{3+}, 2, and 1^{4+} (cf. Figure 9b). However, they differ from what is obtained from the combination of Gd^{3+}, unsubstituted PTADA, and 1^{4+}. Taken in concert, these findings provide further support for the proposition that the structures of metal-based frameworks produced from the tetracationic host 1^{4+}, lanthanide(III) cations, and PTADA-type anions depend on not only the choice of cation but also the nature of the dianionic guest.

The anion precursor dependence on the structure and emission properties is seen in the multicomponent self-assembly among 1^{4+}, Eu^{3+}, and anion PTADA, 2, 6, or 7. Dianions 6 and 7 were used to test further the extent to which substituent-based precursor differences could affect the above multicomponent, metal-based self-assembly process. Using crystal growth procedures analogous to those used to obtain the 2D MORFs, $[1^{4+}\cdot 2_5\cdot M_2]_n$ (M = Gd^{3+}, Eu^{3+}, Nd^{3+}, Sm^{3+}, Tb^{3+}), a combination of 6 or 7, Eu^{3+}, and 1^{4+} yielded diffraction-quality single crystals of $[1^{4+}\cdot 6_8\cdot Eu^{3+}_4\cdot 4H_2O]\cdot 4H_2O\cdot 3DMF$ and $[1^{4+}\cdot 7_8\cdot Eu^{3+}_4\cdot 6H_2O]\cdot 18.5H_2O$, respectively (cf. Figure 10). In contrast to the MIMs produced with PTADA or 2, where changes in the anion

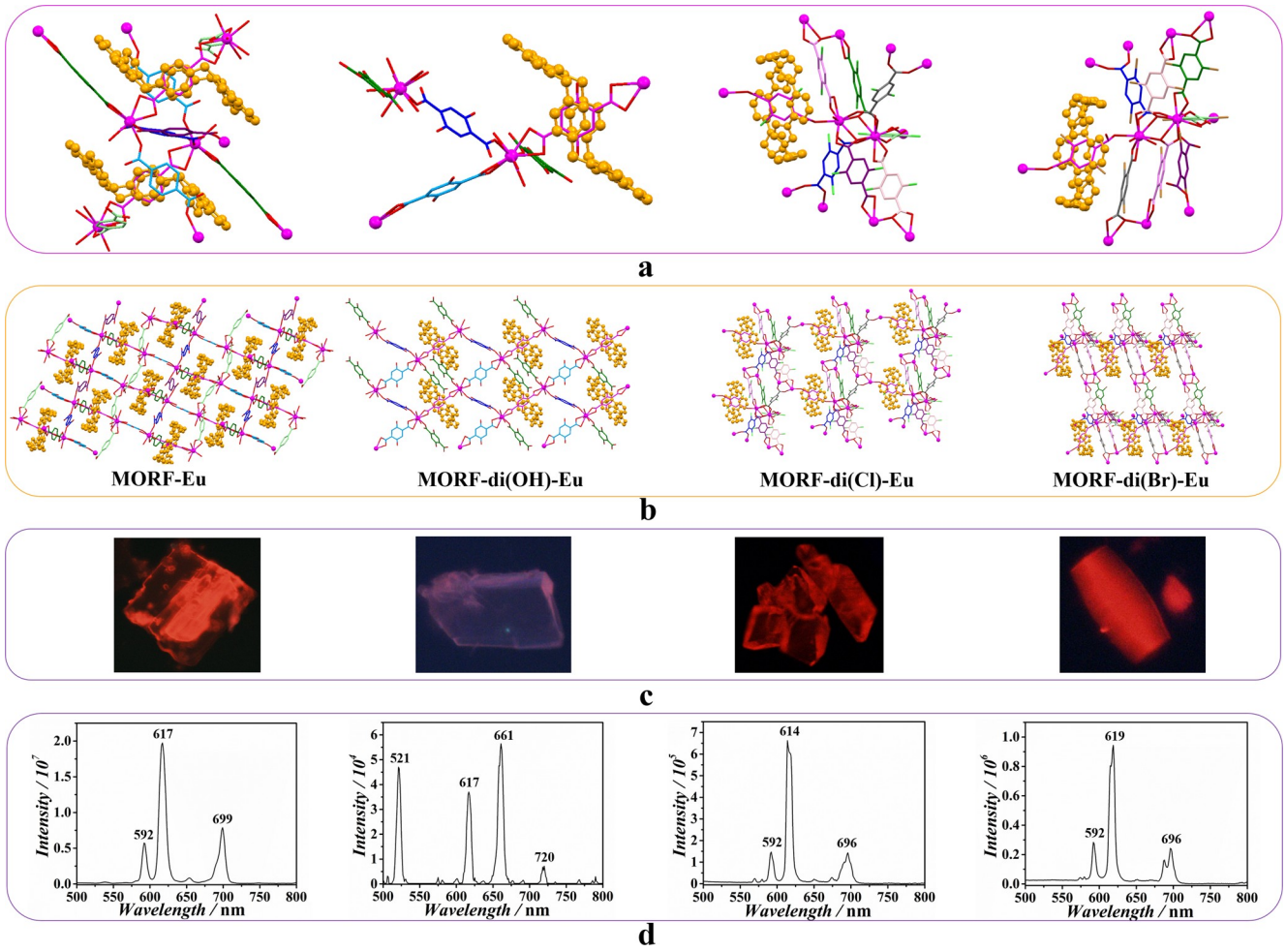

Figure 10. Single-crystal X-ray structures (a) and 3D-framework structures (b) of $[1^{4+}\cdot PTADA_5\cdot Eu^{3+}_2\cdot 3H_2O]_n$, $[1^{4+}\cdot 2_5\cdot Eu^{3+}_2\cdot 6H_2O]_n$, $[1^{4+}\cdot 6_8\cdot Eu^{3+}_4\cdot 4H_2O]_n$, $[1^{4+}\cdot 7_8\cdot Eu^{3+}_4\cdot 6H_2O]_n$, $[1^{4+}\cdot PTADA_5\cdot Eu^{3+}_2\cdot 3H_2O]\cdot 16H_2O$ (MORF-Eu), $[1^{4+}\cdot 2_5\cdot Eu^{3+}_2\cdot 6H_2O]\cdot 4H_2O\cdot 4DMF$ (MORF-di(OH)-Eu), $[1^{4+}\cdot 6_8\cdot Eu^{3+}_4\cdot 4H_2O]\cdot 4H_2O\cdot 3DMF$ (MORF-di(Cl)-Eu), and $[1^{4+}\cdot 7_8\cdot Eu^{3+}_4\cdot 6H_2O]\cdot 18.5H_2O$ (MORF-di(Br)-Eu) as determined via single-crystal X-ray diffraction analyses. All metal atoms are shown as blue balls. Different colors are used to highlight the different local chemical environments of the various linking anions. Luminescence microscopic photos (c) of each single crystal in (a) under conditions of 365 nm illumination. (d) Solid photoluminescence spectra of each single crystal in (a) obtained using an excitation wavelength of 424 nm.

https://dx.doi.org/10.1021/jacs.9b13473
J. Am.Chem. Soc. 2020, 142, 7443−7455

conformation and binding orientation are seen in the presence of M, in the case of the MIMs derived from 6 or 7 similar interpenetrated binding modes are found in the absence or presence of the Eu^{3+} metal cation. Specifically, the benzene ring of the anionic guest adopts a near-vertical orientation with respect to the benzene bridge present in 1^{4+}. Moreover, in contrast to what was found in the 2D MORFs produced with PTADA or 2 and various lanthanide(III) cations, the Eu^{3+} centers in $[1^{4+}\cdot 6_8\cdot Eu^{3+}_4\cdot 4H_2O]\cdot 4H_2O\cdot 3DMF$ and $[1^{4+}\cdot 7_8\cdot Eu^{3+}_4\cdot 6H_2O]\cdot 18.5H_2O$ serve to link dimeric structures, producing ultimately 3D MORF-type constructs.

The emissive features of the higher-order self-assemblies produced from various combinations of Eu^{3+}, 1^{4+}, and PTADA and its derivatives were also found to depend on the choice of anionic guest. These differences are readily apparent to the unaided eye in that different colors are seen for crystals of $[1^{4+}\cdot PTADA_5\cdot Eu^{3+}_2\cdot 3H_2O]_n$, $[1^{4+}\cdot 2_5\cdot Eu^{3+}_2\cdot 6H_2O]_n$, $[1^{4+}\cdot 6_8\cdot Eu^{3+}_4\cdot 4H_2O]_n$, and $[1^{4+}\cdot 7_8\cdot Eu^{3+}_4\cdot 6H_2O]_n$ on excitation with 365 nm light (cf. Figure 10 and Figure S109 in the Supporting Information). The differences in the corresponding emission spectra, including the peak wavelength, $\lambda_{Em.max}$, and the lifetime, τ, are summarized in Table 6. The underlying data are included in the Supporting Information (cf. Section S11).

Table 6. Fluorescence Features Determined for Crystalline Samples of $[1^{4+}\cdot PTADA_5\cdot Eu^{3+}_2\cdot 3H_2O]_n$, $[1^{4+}\cdot 2_5\cdot Eu^{3+}_2\cdot 6H_2O]_n$, $[1^{4+}\cdot 6_8\cdot Eu^{3+}_4\cdot 4H_2O]_n$, and $[1^{4+}\cdot 7_8\cdot Eu^{3+}_4\cdot 6H_2O]_n$

crystal	$\lambda_{Em.max}$ (nm)	τ (μs)
$[1^{4+}\cdot PTADA_5\cdot Eu^{3+}_2\cdot 3H_2O]_n$	617	1246
$[1^{4+}\cdot 2_5\cdot Eu^{3+}_2\cdot 6H_2O]_n$	661	199
$[1^{4+}\cdot 6_8\cdot Eu^{3+}_4\cdot 4H_2O]_n$	614	573.1
$[1^{4+}\cdot 7_8\cdot Eu^{3+}_4\cdot 6H_2O]_n$	619	701.6

Particularly notable differences are seen in the $\lambda_{Em.max}$ value of $[1^{4+}\cdot 2_5\cdot Eu^{3+}_2\cdot 6H_2O]_n$ relative to the other three structures. Complexes $[1^{4+}\cdot PTADA_5\cdot Eu^{3+}_2\cdot 3H_2O]_n$, $[1^{4+}\cdot 6_8\cdot Eu^{3+}_4\cdot 4H_2O]_n$, and $[1^{4+}\cdot 7_8\cdot Eu^{3+}_4\cdot 6H_2O]_n$ give rise to an intense red luminescence upon excitation at 365 nm. Their emission spectra are characterized by three intense features centered at 592 nm, at around 617 nm, and at around 696 nm (λ_{Ex} = 424 nm) that are assigned to $^5D_0 \rightarrow {}^7F_1$, $^5D_0 \rightarrow {}^7F_2$, and $^5D_0 \rightarrow {}^7F_4$ transitions, respectively. In contrast, under 365 nm UV light, $[1^{4+}\cdot 2_5\cdot Eu^{3+}_2\cdot 6H_2O]_n$ appears purple to the naked eye. The emission spectrum of this complex includes bands at 621, and 720 nm (λ_{Ex} = 424 nm), respectively, that are ascribed to $^5D_0 \rightarrow {}^7F_3$, $^5D_0 \rightarrow {}^7F_3$, and $^5D_0 \rightarrow {}^7F_4$ transitions, respectively. This complex also had the smallest τ value. The unique nature of $[1^{4+}\cdot 2_5\cdot Eu^{3+}_2\cdot 6H_2O]_n$ leads us to propose that, as a consequence of an −OH substituent effect,[15] there is effective energy transfer from the ligand 2 to the Eu^{3+} center ion in this complex that is not seen in the case of the corresponding species prepared from PTADA, 6, or 7. More broadly, this combination of findings serves to underscore further how small differences in the anionic guest can translate into readily discernible differences in the bulk properties of self-assembled complexes generated under ostensibly identical conditions.

CONCLUSION

In summary, we have shown here how modest changes in the substituent on a PTADA core can influence the interaction of such anionic precursors with the cation macrocycle 1^{4+}. Monosubstituted or para-disubstituted derivatives bearing relatively small substituents (e.g., 2-OH, 2,5-di(OH), 2,5-di(NH_2), 2,5-di(Me), 2,5-di(Cl), 2,5-di(Br), or 2,5-di(I)) support the formation of pseudorotaxane structures when they are combined with 1^{4+}. In contrast, PTADA itself and its 2,3-di(OH), 2,6-di(OH), and 2,3,5,6-tetra(Cl) derivatives give rise to complexes characterized by so-called outside binding when they are allowed to interact with 1^{4+}. A combination of steric, electronic, and intramolecular hydrogen-bonding effects within the PTADA derivatives is thought to dictate which binding mode prevails. Dianionic guest substituent effects are also manifested in terms of dictating structures whose complexity extends beyond the first coordination sphere. For instance, the introduction of a specific substituent (2,5-di(OH)) on the PTADA core (to give 2) serves to convert formally PTADA containing complexes characterized by extended self-assembly ($M = Ni^{2+}$, Co^{2+}, Zn^{2+}, Cd^{2+}) into polyrotaxane structures. We have also found that the tetra(F) PTADA derivative (13), stabilizes an unusual anionic MOF, wherein the cationic 1^{4+} is included into the hole of the MOF on crystallization under standard conditions. Likewise, the use of 2 in lieu of PTADA serves to convert the RSOF ($M = Gd^{3+}$) for 3D MORFs ($M = Eu^{3+}$, Nd^{3+}, Sm^{3+}, Tb^{3+}) seen with PTADA into new 2D MORFs ($M = Gd^{3+}$, Eu^{3+}, Nd^{3+}, Sm^{3+}, Tb^{3+}). In addition, it was found that, when PTADA and its 2,5-di(OH), 2,5-di(Cl), and 2,5-di(Br) substituted derivatives (i.e., 2, 6, or 7) are combined with 1^{4+} and Eu^{3+}, MORFs are produced that are characterized by different structural and fluorescence features. We thus propose that a modest variation in the guest substitution patterns could emerge as a useful means of controlling structure over a variety of length scales, including those that extend beyond the initial host−guest recognition and cation coordination spheres. To the extent this proves true, it could allow a useful approach to the preparation of complex MIMs with novel luminescent or functional features.

ASSOCIATED CONTENT

* Supporting Information

The Supporting Information is available free of charge at https://pubs.acs.org/doi/10.1021/jacs.9b13473.

Experimental details, NMR spectroscopic analyses, ESI-HRMS results, data fitting, and single-crystal X-ray diffraction studies (PDF)

Crystallographic data (CIF)
Crystallographic data (CIF)
Crystallographic data (CIF)
Crystallographic data (CIF)
Crystallographic data (CIF)
Crystallographic data (CIF)
Crystallographic data (CIF)
Crystallographic data (CIF)
Crystallographic data (CIF)
Crystallographic data (CIF)
Crystallographic data (CIF)
Crystallographic data (CIF)
Crystallographic data (CIF)
Crystallographic data (CIF)
Crystallographic data (CIF)
Crystallographic data (CIF)
Crystallographic data (CIF)
Crystallographic data (CIF)
Crystallographic data (CIF)
Crystallographic data (CIF)
Crystallographic data (CIF)
Crystallographic data (CIF)
Crystallographic data (CIF)
Crystallographic data (CIF)

https://dx.doi.org/10.1021/jacs.9b13473
J. Am. Chem. Soc. 2020, 142, 7443−7455

Crystallographic data (CIF)
Crystallographic data (CIF)
Crystallographic data (CIF)
Crystallographic data (CIF)
Crystallographic data (CIF)
Crystallographic data (CIF)
Crystallographic data (CIF)
Structures of In1, In2, Out1, and Out2 (ZIP)
Structures of Guest_Co(II), Guest_Ni(II), and Guest_Zn(II) (ZIP)
Structures of Host_Guest_Co(II), Host_Guest_Ni(II), and Host_Guest_Zn(II) (ZIP)

AUTHOR INFORMATION

Corresponding Authors

Jonathan L. Sessler − Department of Chemistry, Shanghai University, Shanghai 200444, People's Republic of China; Department of Chemistry, The University of Texas at Austin, Austin, Texas 78712-1224, United States; orcid.org/0000-0002-9576-1325; Email: sessler@cm.utexas.edu

Han-Yuan Gong − College of Chemistry, Beijing Normal University, Beijing 100875, People's Republic of China; orcid.org/0000-0003-4168-7657; Email: hanyuangong@bnu.edu.cn

Authors

Xu-Lang Chen − College of Chemistry, Beijing Normal University, Beijing 100875, People's Republic of China; orcid.org/0000-0002-4708-8156

Yun-Jia Shen − College of Chemistry, Beijing Normal University, Beijing 100875, People's Republic of China

Chao Gao − College of Chemistry, Beijing Normal University, Beijing 100875, People's Republic of China

Jian Yang − College of Chemistry, Beijing Normal University, Beijing 100875, People's Republic of China

Xin Sun − College of Chemistry, Beijing Normal University, Beijing 100875, People's Republic of China

Xin Zhang − College of Chemistry, Beijing Normal University, Beijing 100875, People's Republic of China

Yu-Dong Yang − College of Chemistry, Beijing Normal University, Beijing 100875, People's Republic of China

Gong-Ping Wei − Institute of Chemistry, Chinese Academy of Sciences, Beijing 100190, People's Republic of China; University of Chinese Academy of Sciences, Beijing 100049, People's Republic of China

Jun-Feng Xiang − Institute of Chemistry, Chinese Academy of Sciences, Beijing 100190, People's Republic of China; University of Chinese Academy of Sciences, Beijing 100049, People's Republic of China

Complete contact information is available at: https://pubs.acs.org/10.1021/jacs.9b13473

Notes

The authors declare no competing financial interest.

ACKNOWLEDGMENTS

H.-Y.G. is grateful to the National Natural Science Foundation of China (21971022, 21472014, and 21672025), National Basic Research Program of China (973 Program 2015CB856502), the Young One-Thousand-Talents Scheme, the Fundamental Research Funds for the Central Universities, the Beijing Municipal Commission of Education, the Beijing National Laboratory for Molecular Science (BNLMS), and Beijing Normal University for financial support. The work in Austin was supported by the US National Science Foundation (CHE-1807152) and the Robert A. Welch Foundation (F-0018). Support from Shanghai University is also gratefully acknowledged.

REFERENCES

(1) (a) Chen, C. − L.; Chen, Y. − T.; Demchenko, A. P.; Chou, P. − T. Amino Proton Donors in Excited-state Intramolecular Proton-transfer Reactions. Nat. Rev. Chem. 2018, 2, 131−143. (b) Mao, Y.-Z.; Head-Gordon, M.; Shao, Y. − H. Unraveling Substituent Effects on Frontier Orbitals of Conjugated Molecules Using an Absolutely Localized Molecular Orbital Based Analysis. Chem. Sci. 2018, 9, 8598−8607. (c) Suzuki, S.; Yamaguchi, J. Synthesis of fully arylated (hetero)arenes. Chem. Commun. 2017, 53, 1568−1582. (d) Ni, C. − F.; Hu, J. − B. The Unique Fluorine Effects in Organic Reactions: Recent Facts and Insights into Fluoroalkylations. Chem. Soc. Rev. 2016, 45, 5441−5454. (e) Ogoshi, T.; Yamagishi, T.; Nakamoto, Y. Pillar-Shaped Macrocyclic Hosts Pillar[n]arenes: New Key Players for Supramolecular Chemistry. Chem. Rev. 2016, 116, 7937−8002. (f) Preshlock, S.; Tredwell, M.; Gouverneur, V. ^{18}F-Labeling of Arenes and Heteroarenes for Applications in Positron Emission Tomography. Chem. Rev. 2016, 116, 719−766. (g) Wu, C.-H.; Galabov, B.; Wu, J. I-C.; Ilieva, S.; Schleyer, P. R.; Allen, W. D. Do π-Conjugative Effects Facilitate S$_N$2 Reactions? J. Am. Chem. Soc. 2014, 136, 3118−3126. (h) Galabov, B.; Ilieva, S.; Koleva, G.; Allen, W. D.; Schaefer, H. F., III; Schleyer, P. R. Structure−reactivity Relationships for Aromatic Molecules: Electrostatic Potentials at Nuclei and Electrophile Affinity Indices. WIREs Comput. Mol. Sci. 2013, 3, 37−55. (i) Wheeler, S. Understanding Substituent Effects in Noncovalent Interactions Involving Aromatic Rings. Acc. Chem. Res. 2013, 46, 1029−1038.

(2) (a) Dhakshinamoorthy, A.; Li, Z. − H.; Garcia, H. Catalysis and Photocatalysis by Metal Organic Frameworks. Chem. Soc. Rev. 2018, 47, 8134−8172. (b) Su, T. A.; Neupane, M.; Steigerwald, M. L.; Venkataraman, L.; Nuckolls, C. Chemical Principles of Single-molecule Electronics. Nat. Rev. Mater. 2016, 1, 16002. (c) Yu, X.-P.; Jia, J. − T.; Xu, S.; Lao, K. U.; Sanford, M. J.; Ramakrishnan, R. K.; Nazarenko, S. I.; Hoye, T. R.; Coates, G. W.; DiStasio, R. A., Jr. Unraveling Substituent Effects on the Glass Transition Temperatures of Biorenewable Polyesters. Nat. Commun. 2018, 9, 2880.

(3) (a) Shao, B.-H.; Qian, H.; Li, Q.; Aprahamian, I. Structure Property Analysis of the Solution and Solid-State Properties of Bistable Photochromic Hydrazones. J. Am. Chem. Soc. 2019, 141, 8364−8371. (b) Chan, A. K. − W.; Ng, M.; Low, K.-H.; Yam, V. W. − W. Versatile Control of Directed Supramolecular Assembly via Subtle Changes of the Rhodium(I) Pincer Building Blocks. J. Am. Chem. Soc. 2018, 140, 8321−8329. (c) Xu, L. -N; Shen, X.; Zhou, Z.-X.; He, T.; Zhang, J. − J.; Qiu, H.-Y.; Saha, M. L.; Yin, S.− C.; Stang, P. J. Metallacycle-Cored Supramolecular Polymers: Fluorescence Tuning by Variation of Substituents. J. Am. Chem. Soc. 2018, 140, 16920−16924. (d) He, Q.; Tu, P.; Sessler, J. L. Supramolecular Chemistry of Anionic Dimers, Trimers, Tetramers, and Clusters. Chem. 2018, 4, 46−93. (e) Riwar, L. − J.; Trapp, N.; Kuhn, B.; Diederich, F. Substituent Effects in Parallel-Displaced π−π Stacking Interactions: Distance Matters. Angew. Chem., Int. Ed. 2017, 56, 11252−11257. (f) Suzuki, M.; Juliet, F.; Kotyk, K.; Khan, S. I.; Rubin, Y. Directing the Crystallization of Dehydro[24]-annulenes into Supramolecular Nanotubular Scaffolds. J. Am. Chem. Soc. 2016, 138, 5939−5956. (g) Zhang, Y.; Zhan, T.-G.; Zhou, T. − Y.; Qi, Q. − Y.; Xu, X − N.; Zhao, X. Fluorescence enhancement through the formation of a single-layer two-dimensional supramolecular organic framework and its application in highly selective recognition of picric acid. Chem. Commun. 2016, 52, 7588−7591. (h) Feng, Y.; Chen, H.; Liu, Z. − X.; He, Y. − M.; Fan, Q. − H. A Pronounced Halogen Effect on the Organogelation Properties of Peripherally Halogen Functionalized Poly(benzyl ether) Dendrons. Chem. − Eur. J. 2016, 22, 4980−4990. (i) Pan, F. − F.; Beyeh, N. K.; Rissanen, K. Concerted Halogen-Bonded Networks with N-Alkyl Ammonium Resorcinarene Bromides:

https://dx.doi.org/10.1021/jacs.9b13473
J. Am. Chem. Soc. 2020, 142, 7443−7455

From Dimeric Dumbbell to Capsular Architecture. J. Am. Chem. Soc. 2015, 137, 10406−10413. (j) Tresca, B. W.; Hansen, R. J.; Chau, C. V.; Hay, B. P.; Zakharov, L. N.; Haley, M. M.; Johnson, D. W. Substituent Effects in CH Hydrogen Bond Interactions: Linear Free Energy Relationships and Influence of Anions. J. Am. Chem. Soc. 2015, 137, 14959−14967. (k) Li, Y. − J.; Flood, A. H. Strong, Size-Selective, and Electronically Tunable C-H···Halide Binding with Steric Control over Aggregation from Synthetically Modular, Shape-Persistent [8$_4$]-Triazolophanes. J. Am. Chem. Soc. 2008, 130, 12111−12122.

(4) (a) Lavendomme, R.; Ronson, T. K.; Nitschke, J. R. Metal and Organic Templates Together Control the Size of Covalent Macrocycles and Cages. J. Am. Chem. Soc. 2019, 141, 12147−12158. (b) McTernan, C. T.; Ronson, T. K.; Nitschke, J. R. Post-assembly Modification of Phosphine Cages Controls Host−Guest Behavior. J. Am. Chem. Soc. 2019, 141, 6837−6842. (c) Carpenter, J. P.; McTernan, C. T.; Ronson, T. K.; Nitschke, J. R. Anion Pairs Template a Trigonal Prism with Disilver Vertices. J. Am. Chem. Soc. 2019, 141, 11409−11413. (d) Zhang, W.-Y.; Yang, D.; Zhao, J.; Hou, L.-K.; Sessler, J. L.; Yang, X.-J.; Wu, B. Controlling the Recognition and Reactivity of Alkyl Ammonium Guests Using an Anion Coordination-Based Tetrahedral Cage. J. Am. Chem. Soc. 2018, 140, 5248−5256. (e) Fujita, D.; Ueda, Y.; Sato, S.; Yokoyama, H.; Mizuno, N.; Kumasaka, T.; Fujita, M. Self-Assembly of $M_{30}L_{60}$ Icosidodecahedron. Chem. 2016, 1, 91−101. (f) Ousaka, N.; Grunder, S.; Castilla, A. M.; Whalley, A. C.; Stoddart, J. F.; Nitschke, J. R. Efficient Long-Range Stereochemical Communication and Cooperative Effects in Self-Assembled L_4L_6 Cages. J. Am. Chem. Soc. 2012, 134, 15528−15537. (g) Sun, Q.-F.; Iwasa, J.; Ogawa, D.; Ishido, Y.; Sato, S.; Ozeki, T.; Sei, Y.; Yamaguchi, K.; Fujita, M. Self-Assembled $M_{24}L_{48}$ Polyhedra and Their Sharp Structural Switch upon Subtle Ligand Variation. Science 2010, 328, 1144−1147.

(5) Klosterman, J. K.; Yamauchi, Y.; Fujita, M. Engineering discrete stacks of aromatic molecules. Chem. Soc. Rev. 2009, 38, 1714−1725.

(6) (a) Furukawa, H.; Muller, U.; Yaghi, O. M. "Heterogeneity within Order" in Metal−Organic Frameworks. Angew. Chem., Int. Ed. 2015, 54, 3417−3430. (b) Li, M.; Li, D.; O'Keeffe, M.; Yaghi, O. M. Topological Analysis of Metal−Organic Frameworks with Polytopic Linkers and/or Multiple Building Units and the Minimal Transitivity Principle. Chem. Rev. 2014, 114, 1343−1370.

(7) (a) Zhao, C.-F.; Diercks, C. S.; Zhu, C.-H.; Hanikel, N.; Pei, X.-K.; Yaghi, O. M. Urea-Linked Covalent Organic Frameworks. J. Am. Chem. Soc. 2018, 140, 16438−16441. (b) Liu, Y.-Z.; Ma, Y.-H.; Yang, J.-J.; Diercks, C. S.; Tamura, N.; Jin, F.-Y.; Yaghi, O. M. Molecular Weaving of Covalent Organic Frameworks for Adaptive Guest Inclusion. J. Am. Chem. Soc. 2018, 140, 16015−16019. (c) Waller, P. J.; AlFaraj, Y. S.; Diercks, C. S.; Jarenwattananon, N. N.; Yaghi, O. M. Conversion of Imine to Oxazole and Thiazole Linkages in Covalent Organic Frameworks. J. Am. Chem. Soc. 2018, 140, 9099−9103.

(8) (a) Chang, Y. − C.; Jiao, Y.; Symons, H. E.; Xu, J.-F.; Faul, C. F. J.; Zhang, X. Molecular engineering of polymeric supra-amphiphiles. Chem. Soc. Rev. 2019, 48, 989−1003. (b) Lewis, J. E. M.; Beer, P. D.; Loeb, S. J.; Goldup, S. M. Metal ions in the synthesis of interlocked molecules and materials. Chem. Soc. Rev. 2017, 46, 2577−2591. (c) Vukotic, V. N.; O'Keefe, C. A.; Zhu, K. − L.; Harris, K. J.; To, C. T.; Schurko, R. W.; Loeb, S. J. Mechanically Interlocked Linkers inside Metal-Organic Frameworks: Effect of Ring Size on Rotational Dynamics. J. Am. Chem. Soc. 2015, 137, 9643−9651. (d) Yang, L. − L.; Tan, X. − X.; Wang, Z. − Q.; Zhang, X. Supramolecular Polymers: Historical Development, Preparation, Characterization, and Functions. Chem. Rev. 2015, 115, 7196−7239. (e) Qu, D. − H.; Wang, Q. − C.; Zhang, Q. − W.; Ma, X.; Tian, H. Photoresponsive Host-Guest Functional Systems. Chem. Rev. 2015, 115, 7543−7588. (f) Li, S. R.; Zhang, H. − Y.; Xu, X. F.; Liu, Y. Mechanically selflocked chiral gemini-catenanes. Nat. Commun. 2015, 6, 7590. (g) Vukotic, V. N.; Loeb, S. J. Coordination polymers containing rotaxane linkers. Chem. Soc. Rev. 2012, 41, 5896−5906. (h) He, M. − L.; Chen, L. − J.; Jiang, B.; Tan, H. − W.; Wang, C. − H.; Yang, H. − B. Facile construction of Zn(II)-porphyrin-cored [5]rotaxane and its controllable aggregation behaviours. Chin. Chem. Lett. 2019, 30, 131−134. (i) Lim, J. Y. C.; Beer, P. D. Electrochemical Bromide Sensing with a Halogen Bonding [2]-Rotaxane. Eur. J. Org. Chem. 2019, 2019, 3433−3441. (j) Chen, Y.; Guan, F.-H.; Li, Z.-T.; Liu, Y. Controllable macrocyclic supramolecular assemblies in aqueous solution. Chin. Chem. 2018, 61, 979−992. (k) Wang, M. − X. Coronarenes: recent advances and perspectives on macrocyclic and supramolecular chemistry. Sci. China: Chem. 2018, 61, 993−1003. (l) Chen, G. − S.; Jiang, M. Cyclodextrin-based inclusion complexation bridging supramolecular chemistry and macromolecular self-assembly. Chem. Soc. Rev. 2011, 40, 2254−2266.

(9) (a) Corra, S.; de Vet, C.; Groppi, J.; La Rosa, M.; Silvi, S.; Baroncini, M.; Credi, A. Chemical On/Off Switching of Mechanically Planar Chirality and Chiral Anion Recognition in a [2]Rotaxane Molecular Shuttle. J. Am. Chem. Soc. 2019, 141, 9129−9133. (b) Bunchuay, T.; Docker, A.; Martinez-Martinez, A. J.; Beer, P. D. A Potent Halogen-Bonding Donor Motif for Anion Recognition and Anion Template Mechanical Bond Synthesis. Angew. Chem., Int. Ed. 2019, 58, 13823−13827. (c) Wang, Q.-C.; Chen, D. − Z.; Tian, H. Artificial molecular machines that can perform work. Sci. China: Chem. 2018, 61, 1261−1273. (d) Wu, R. − T.; Chi, X.-D.; Hirao, T.; Lynch, V. M.; Sessler, J. L. Supramolecular Properties of a Monocarboxylic Acid-Functionalized "Texas-Sized" Molecular Box. J. Am. Chem. Soc. 2018, 140, 6823−6831. (e) Stoddart, J. F. Mechanically Interlocked Molecules (MIMs)-Molecular Shuttles, Switches, and Machines (Nobel Lecture). Angew. Chem., Int. Ed. 2017, 56, 11094−11125. (f) Gómez-Durán, C. F. A.; Liu, W. − Q.; Betancourt-Mendiola, M. D.; Smith, B. D. Structural Control of Kinetics for Macrocycle Threading by Fluorescent Squaraine Dye in Water. J. Org. Chem. 2017, 82, 8334−8344. (g) Ishiwari, F.; Nakazono, K.; Koyama, Y.; Takata, T. Induction of Single-Handed Helicity of Polyacetylenes Using Mechanically Chiral Rotaxanes as Chiral Sources. Angew. Chem., Int. Ed. 2017, 56, 14858−14862. (h) Yu, G. − C.; Wu, D.; Li, Y.; Zhang, Z. − H.; Shao, L.; Zhou, J.; Hu, Q. − L.; Tang, G. P.; Huang, F. − H. A pillar[5]arene-based [2]rotaxane lights up mitochondria. Chem. Sci. 2016, 7, 3017−3024. (i) Chen, Q. − H.; Sun, J. L.; Li, P.; Hod, I.; Moghadam, P. Z.; Kean, Z. S.; Snurr, R. Q.; Hupp, J. T.; Farha, O. K.; Stoddart, J. F. A Redox-Active Bistable Molecular Switch Mounted inside a Metal-Organic Framework. J. Am. Chem. Soc. 2016, 138, 14242−14245. (j) Leung, K. C.-F.; Wong, W.-Y.; Arico, F.; Haussmann, P. C.; Stoddart, J. F. The stability of imine-containing dynamic [2]rotaxanes to hydrolysis. Chem. Commun. 2010, 8, 83−89. (k) Liu, Y.; Flood, A. H.; Moskowitz, R. M.; Stoddart, J. F. Versatile Self-Complexing Compounds Based on Covalently Linked Donor−Acceptor Cyclophanes. Chem. - Eur. J. 2005, 11, 369−385.

(10) Considerable work, both theoretical and experimental, has been devoted to exploring substituent effects in the context of anion binding. However, most of this effort has involved the effect of substituents present on the ligand (receptor), not on the anion per se as in the present study. Selected reports on prior substituent effect studies include the following: (a) Helttunen, k.; Annala, R.; Suhonen, A.; Iloniemi, J.; Kalenius, E.; Aragay, G.; Ballester, P.; Tuononen, H. M.; Nissinen, M. Oligoamide Foldamers as Helical Chloride Receptors: the Influence of Electron-Withdrawing Substituents on Anion-Binding Interactions. Chem. - Asian J. 2019, 14, 647−654. (b) Gale, P. A.; Howe, E. N.W.; Wu, X. Anion Receptor Chemistry. Chem. 2016, 1, 351−422. (c) Tresca, B. W.; Hansen, R. J.; Chau, C. V.; Hay, B. P.; Zakharov, L. N.; Haley, M. M.; Johnson, D. W. Substituent Effects in CH Hydrogen Bond Interactions: Linear Free Energy Relationships and Influence of Anions. J. Am. Chem. Soc. 2015, 137, 14959−14967. (d) Nepal, B.; Scheiner, S. Substituent Effects on the Binding of Halides by Neutral and Dicationic Bis(triazolium) Receptors. J. Phys. Chem. A 2015, 119, 13064−13073. (e) Tropiano, M.; Blackburn, O. A.; Tilney, J. A.; Hill, L. R. F.; Placidi, M. P.; Aarons, R. J.; Sykes, D.; Jones, M. W.; Kenwright, A. M.; Snaith, J. S.; Sørensen, T. J.; Faulkner, S. Using Remote Substituents to Control Solution Structure and Anion Binding in Lanthanide Complexes. Chem. - Eur. J. 2013, 19, 16566−16571. (f) Ghosh, A.; Jose, D. A.; Das, A.; Ganguly, B. A density functional study towards substituent effects on anion sensing with urea receptors. J. Mol. Model. 2010, 16, 1441−1448.

(11) (a) Gong, H.-Y.; Rambo, B. M.; Nelson, C. A.; Cho, W.; Lynch, V. M.; Zhu, X.; Oh, M.; Sessler, J. L. Multi Component Self-assembly:

https://dx.doi.org/10.1021/jacs.9b13473
J. Am. Chem. Soc. 2020, 142, 7443−7455

Supramolecular Organic Frameworks Containing Metal-rotaxane Subunits (RSOFs). Dalton Trans. 2012, 41, 1134−1137. (b) Gong, H.-Y.; Rambo, B. M.; Nelson, C. A.; Lynch, V. M.; Zhu, X.; Sessler, J. L. Rare-earth Cation Effects on Three-dimensional Metal-organic Rotaxane Framework (MORF) self-assembly. Chem. Commun. 2012, 48, 10186−10188. (c) Gong, H.-Y.; Rambo, B. M.; Cho, W.; Lynch, V. M.; Oh, M.; Sessler, J. L. Anion-directed Assembly of a Three-dimensional Metal-organic Rotaxane Framework. Chem. Commun. 2011, 47, 5973−5975. (d) Gong, H.-Y.; Rambo, B. M.; Karnas, E.; Lynch, V. M.; Sessler, J. L. A 'Texas-sized' Molecular Box that Forms an Anion-induced Supramolecular Necklace. Nat. Chem. 2010, 2, 406−409.

(12) Sun, Y.-R.; Gu, J.; Wang, H.-Y.; Sessler, J. L.; Thordarson, P.; Lin, Y.-J.; Gong, H.-G. AAAA-DDDD Quadruple H-Bond-Assisted Ionic Interactions: Robust Bis(Guanidinium)/DiCarboxylate Heteroduplexes in Water. J. Am. Chem. Soc. 2019, 141, 20146.

(13) (a) Yang, Y.-D.; Sessler, J. L.; Gong, H.-Y. Flexible imidazolium macrocycles: building blocks for anion-induced self-assembly. Chem. Commun. 2017, 53, 9684−9696. (b) Anioła, M.; Dega-Szafran, Z.; Katrusiak, A.; Komasa, A.; Szafran, M. Disproportional proton tautomers of pipecolic acid and 2,6-dichloro-4-nitrophenol in 2:3 complex. Chem. Phys. 2016, 477, 88−95. (c) Takashima, Y.; Sakamoto, K.; Oizumi, Y.; Yamaguchi, H.; Kamitori, S.; Harada, A. J. Inclusion Phenom. Mol. Recogn. Chem. 2006, 56, 45−53. (d) Katoh, M.; Kohmoto, S.; Kishikawa, K. A hexagonal columnar packing structure of C7 symmetric supramolecules: superstructure of 2:3 complex of heptakis-(6-O-tert-butyl-dimethylsilyl)-β-cyclodextrin and ethyl-eta-tate. Cryst. Res. Technol. 2006, 41, 1242−1245. (e) Kobayashi, T.; Ashida, T.; Uyeda, N.; Suito, E.; Kakudo, M. The Crystal Structure of the 2:3 Complex of Zinc Phthalocyanine and n-Hexylamine. Bull. Chem. Soc. Jpn. 1971, 44, 2095−2103.

(14) (a) Tamang, S. R.; Singh, A.; Bedi, D.; Bazkiaei, A. R.; Warner, A. A.; Glogau, K.; McDonald, C.; Unruh, D. K.; Findlater, M. Polynuclear lanthanide−diketonato clusters for the catalytic hydroboration of carboxamides and esters. Nat. Catal. 2020, 3, 154−162. (b) Zhang, T.; Lin, W.-B. Metal−organic frameworks for artificial photosynthesis and photocatalysis. Chem. Soc. Rev. 2014, 43, 5982−5993. (c) Wang, J.-H.; Zakrzewski, J. J.; Heczko, M.; Zychowicz, M.; Nakagawa, K.; Nakabayashi, K.; Sieklucka, B.; Chorazy, S.; Ohkoshi, S. Proton Conductive Luminescent Thermometer Based on Near Infrared Emissive {YbCo2} Molecular Nanomagnet. J. Am. Chem. Soc. 2020, 142, 3970.

(15) (a) Xiong, J.; Yang, L.; Gao, L.-X.; Zhu, P.-P.; Chen, Q.; Tan, K.-J. A highly fluorescent lanthanide metal-organic framework as dual-mode visual sensor for berberine hydrochloride and tetracycline. Anal. Bioanal. Chem. 2019, 411, 5963−5973. (b) Zhang, S.-R.; Du, D.-Y.; Tan, K.; Qin, J.-S.; Dong, H.-Q.; Li, S.-L.; He, W.-W.; Lan, Y.-Q.; Shen, P.; Su, Z.-M. Self-Assembly versus Stepwise Synthesis: Heterometal−Organic Frameworks Based on Metalloligands with Tunable Luminescence Properties. Chem. Eur. J. 2013, 19, 11279−11286.

https://dx.doi.org/10.1021/jacs.9b13473
J. Am. Chem. Soc. 2020, 142, 7443−7455